DMD Fast Forward. Published on July 6, 2018 as DOI: 10.1124/dmd.118.081182
This article has not been copyedited and formatted. The final version may differ from this version.

DMD # 81182

Title

Differences of the *in vivo* and *in vitro* metabolism of imrecoxib in humans: formation of rate-limiting aldehyde intermediate

Xiangyu Hou, Jialan Zhou, Songda Yu, Lei Zhou, Yifan Zhang, Dafang Zhong, Xiaoyan Chen

Shanghai Institute of Materia Medica, Chinese Academy of Sciences, 501 Haike Road, Shanghai 201203, P.R. China (X.H., J.Z., S.Y., L.Z., Y.Z., D.Z., X.C.)

University of Chinese Academy of Sciences, No.19A Yuquan Road, Beijing 100049, China (X.H., D.Z., X.C.)

DMD Fast Forward. Published on July 6, 2018 as DOI: 10.1124/dmd.118.081182
This article has not been copyedited and formatted. The final version may differ from this version.

Running Title: Differences of the *in vivo* and *in vitro* metabolism of imrecoxib

Corresponding Author:

Xiaoyan Chen

Shanghai Institute of Materia Medica, Chinese Academy of Sciences, 501 Haike Road, Shanghai, 201203, China;

Phone: +86-21-50800738; Fax: 0086-21-50800738;

Email: xychen@simm.ac.cn

Number of text pages: 20

Number of tables: 1

Number of figures: 9

Number of references: 32

Number of words in the Abstract: 242

Number of words in the Introduction: 290

Number of words in the Discussion: 1281

Abbreviations: ABT, 1-aminobenzotriazole; ADH, alcohol dehydrogenase; ALDH, aldehyde dehydrogenase; AOX, aldehyde oxidase; COX-2, cyclooxygenase-2; CYP, cytochrome P450; DCM, dichloromethane; DDI, drug-drug interaction; DMSO, dimethyl sulfoxide; DOPAL, 3,4-dihydroxyphenylacetaldehyde; ESI, electrospray ionization; ETC, electron transport chain; FAD, flavin adenine dinucleotide; Hepa, human hepatocytes; HLC, human liver cytosol; HLM, human liver microsomes; HPLC, high-performance liquid chromatography; IDA, information-dependent acquisition; IS, internal standard; M-CHO, aldehyde imrecoxib; MRM, multiple reaction monitoring; MS, mass spectrometry; NAD, nicotinamide adenine dinucleotide; NADP, nicotinamide adenine dinucleotide phosphate; NADPH, reduced

DMD Fast Forward. Published on July 6, 2018 as DOI: 10.1124/dmd.118.081182
This article has not been copyedited and formatted. The final version may differ from this version.

form of nicotinamide adenine dinucleotide phosphate; NMR, nuclear magnetic resonance; NSAIDs, nonsteroidal anti-inflammatory drugs; PBS, phosphate-buffered saline; POR, CYP reductase; Q-TOF/MS, quadrupole time-of-flight mass spectrometry; UPLC, ultra-performance liquid chromatography; UV, ultraviolet; WME, Williams' E medium; XO, xanthine oxidase.

DMD Fast Forward. Published on July 6, 2018 as DOI: 10.1124/dmd.118.081182
This article has not been copyedited and formatted. The final version may differ from this version.

ABSTRACT

Imrecoxib is a typical cyclooxygenase-2 inhibitor and the benzylic carbon motif is its major site of oxidative metabolism, producing a hydroxymethyl metabolite (M1) and a carboxylic acid metabolite (M2). The plasma exposure of M2 is both four times higher than those of M0 and M1 in humans. However, this metabolite is rarely formed in *in vitro* experiments. Therefore, the present study aims to investigate the formation mechanism of M2, and to further elucidate the reason for the discrepancy between *in vitro* and *in vivo* metabolic data. By employing human hepatocytes, human liver microsomes (HLM), human liver cytosols (HLC), recombinant enzymes, and selective enzyme inhibitors, the metabolic map of imrecoxib was elaborated as follows: the parent drug was initially hydroxylated to form M1 in HLM, mainly mediated by CYP3A4 and CYP2D6; and subsequently form aldehyde imrecoxib (M-CHO) in HLM and HLC. The latter process is the rate-limiting step in generating the end-product M2. In further M-CHO metabolism, two opposite reactions namely, rapid oxidation catalyzed by CYP3A4, CYP2D6, and cytosolic aldehyde oxidase to form M2 versus reduction to regenerate M1 mediated by NADPH-dependent reductases in HLM and HLC, such as cytochrome P450 reductase, led to marked underestimation of the M2 amount in static *in vitro* incubations. The findings provided a possible explanation for the difference between *in vitro* and *in vivo* metabolism of imrecoxib, suggesting that the effect of competitive reduction on the static oxidation metabolism in *in vitro* metabolic experiments should be considered.

Introduction

Coxibs are widely used in clinical practice as nonsteroidal anti-inflammatory drugs for alleviating pain based on its inhibition of cyclooxygenase-2 (COX-2). Typical marketed coxibs, such as celecoxib and etoricoxib, both contain the aromatic methyl group, which is their major site of oxidative metabolism, producing a hydroxymethyl metabolite with subsequent oxidation to the corresponding carboxylic acid metabolite (Paulson et al., 2000; Rodrigues et al., 2003). CYP2C9 is reportedly involved in the formation of hydroxymethyl celecoxib (Tang et al., 2000; Tang et al., 2001), and alcohol dehydrogenase (ADH) is responsible for further metabolism to carboxy-celecoxib (Sandberg et al., 2002).

Similar to celecoxib, imrecoxib, another moderately selective COX-2 inhibitor approved in 2011, also contains a *para*-benzyl fraction. The metabolism of imrecoxib in rats has been investigated (Xu et al., 2006a; Xu et al., 2006b). It undergoes a two-step oxidation of benzylic carbon and successively forms hydroxymethyl metabolite (M1) and carboxylic acid metabolite (M2), which are both confirmed to exhibit similar pharmacological activity to the parent drug (Feng et al., 2009). However, the metabolism of imrecoxib in humans has not been reported.

The design of drug-drug interaction (DDI) clinical trials is essential for the clinical use of imrecoxib. Thus, understanding the principal metabolizing routes and identifying the enzymes involved are of considerable importance. Our pilot experiment indicated that the major metabolites of imrecoxib in humans after an oral administration are M1 and M2 by a two-step successive oxidization. M2 is the prominent drug-related component in both plasma and urine. However, this metabolite is, seldom formed in human liver microsomes (HLMs) in *in vitro* experiments. Therefore, another objective of the study is to explore the formation

DMD Fast Forward. Published on July 6, 2018 as DOI: 10.1124/dmd.118.081182
This article has not been copyedited and formatted. The final version may differ from this version.

mechanism of M2 so as to further elaborate the cause for the discrepancy between *in vitro* and *in vivo* metabolic data.

DMD Fast Forward. Published on July 6, 2018 as DOI: 10.1124/dmd.118.081182
This article has not been copyedited and formatted. The final version may differ from this version.

Materials and methods

Chemicals and reagents. Reference substances of imrecoxib, M1, M2, and BAP385 (internal standard, IS) were kindly provided by Jiangsu Hengrui Medicine Co., Ltd. (Lianyungang, China). Pooled HLM, human liver cytosolic fractions (HLC), and recombinant cytochrome P450 (CYP) enzymes (CYP1A2, 2A6, 2B6, 2C8, 2C9, 2C19, 2D6, 2E1, 3A4, and 3A5, all containing CYP reductase and cytochrome b5) were supplied by BD Gentest (Woburn, MA). Human NADPH-CYP reductase, human CYP3A4R (without cytochrome b5), and human CYP3A4BLR (with cytochrome b5 and low-activity CYP-reductase) were purchased from Cypex Ltd. (Dundee, Scotland, UK). Cryopreserved primary human hepatocytes were obtained from Xeno-Tech (Lenexa, KS, USA). NADPH, NAD, NADP, α-lipoic acid, and 1-aminobenzotriazole (ABT) were purchased from Sigma-Aldrich (St. Louis, MO). References of menadione and methoxyamine were obtained from Meilunbio (Dalian, China). All other reagents and solvents were either analytical or high-performance liquid chromatography (HPLC) grade.

Aldehyde imrecoxib (M-CHO) was synthesized as follows: 1,1-dihydro-1,1,1-triacetoxy-1,2-benzoiodooxol-3(1H)-one (Dess-Martin reagent, 11 mg, 0.026 mmol) was added to a solution of M1 (5 mg, 0.013 mmol) in dichloromethane at 0 °C, and the mixture was stirred for 30 min. Then, the reaction was quenched with $NaHCO_3$-saturated aqueous solution. The organic layer was separated and washed with NaCl saturated aqueous solution, dried over Mg_2SO_4, then filtered and concentrated. The obtained residues were purified with preparative thin-layer chromatography (dichloromethane/methanol = 20:1, v/v) to yield a white solid. The structure was confirmed based on nuclear magnetic resonance (NMR) and mass spectrometry (MS) data. ^{1}H NMR (400 MHz, Chloroform-d) δ 10.03 (s, 1H), 7.92 – 7.85 (m, 4H), 7.58 (d,

DMD Fast Forward. Published on July 6, 2018 as DOI: 10.1124/dmd.118.081182
This article has not been copyedited and formatted. The final version may differ from this version.

J = 8.2 Hz, 2H), 7.45 (d, J = 8.5 Hz, 2H), 4.37 (s, 2H), 3.58 (t, J = 7.4 Hz, 2H), 3.08 (s, 3H), 1.73 (h, J = 7.4 Hz, 2H), 1.01 (t, J = 7.4 Hz, 3H). ^{13}C NMR (126 MHz, Chloroform-d) δ 191.98, 169.39, 146.82, 141.37, 138.49, 137.56, 136.34, 134.74, 130.4 (2C), 130.10 (2C), 128.75 (2C), 128.25 (2C), 52.84, 44.58, 44.56, 22.11, 11.64. HRMS (ESI): *m/z* $[M-H]^-$ calculated for $C_{21}H_{20}NO_4S^-$, 382.1119; found, 382.1120.

Imrecoxib, M1, M-CHO, and other inhibitors were individually prepared by dissolving each compound in dimethyl sulfoxide (DMSO) and diluting with 100 mM phosphate-buffered saline (PBS, pH 7.4) containing $MgCl_2$ (0.5 mM) or Williams' E medium (WME) to the desired concentrations (with a final organic content of 0.1% v/v, except for α-lipoic acid, which required 10% v/v, due to the poor water solubility; the same organic content was retained for the controls).

Instruments. Metabolite profiling was performed on an Acquity UPLC system (Waters Corp., Milford, MA) coupled with a TripleTOF 5600$^+$ system (AB Sciex, Concord, Ontario, Canada). NMR spectra of M-CHO confirmation were recorded on a Bruker Avance III 400 spectrometer (Newark, DE). Quantitation analysis of imrecoxib and its metabolites was conducted using an API 5500 triple quadruple mass spectrometer coupled with a LC-30AD HPLC system (Shimadzu, Kyoto, Japan), and data acquisition and processing were conducted using Analyst 1.6.2 software (AB Sciex).

Animals. Male Sprague-Dawley (SD) rats (200 ± 20 g) were purchased from Sipper-BK laboratory animal Co. Ltd. (Shanghai, China). All animal studies were performed in accordance with the principles of the *Animal Care and Use of Laboratory Committee of the Shanghai Institute of Materia Medica, Chinese Academy of Sciences* (Shanghai, China). The rats were divided into three groups randomly (n = 5/group). Imrecoxib, M1, and M-CHO were intravenously administered separately to each

group at a dose of 5 mg/kg. Then, blood was drawn from the retro-orbital venous before dosing (0 h) and at 5, 15, 30 min, and at 1, 1.5, 2, 4, 7, and 10 h postdosing. Plasma was obtained by centrifugation at 11,000 g for 10 min and stored at -80 °C until analysis.

Human study and sample collection. The study was conducted in accordance with the Helsinki Declaration and the principles of Good Clinical Practice and approved by the Ethics Committee of the Xijing Hospital, affiliated with the Fourth Military Medical University (Xi'an, China). All participants signed informed consents prior to the study. The participants orally received a single dose of 100 mg imrecoxib in fed states. Blood samples were collected before dosing (0 h) and at 0.5, 1, 2, 3, 4, 6, 8, 12, 24, 36, 48, 72, and 96 h postdosing. Plasma was harvested after centrifugation of blood at 11,000 *g* for 10 min. Urine samples were collected predosing (-2-0 h) and at 0-2, 2-4, 4-8, 8-12, 12-24, 24-48, 48-72, and 72-96 h postdose, and the volume of individually collected samples were measured and recorded. Both the plasma and urine samples were stored at -80 °C until analysis.

Sample preparation and ultra-performance liquid chromatography (UPLC)-ultraviolet (UV)/quadrupole time-of-flight mass spectrometry (Q-TOF MS) analysis. An aliquot of 100 μL of sample was mixed with 400 μL of acetonitrile, followed by vortex for 1 min and centrifugation at 14,000 rpm for 5 min. The supernatant was evaporated to dryness under a N_2 stream at 40 °C. The residues were reconstituted with 100 μL of acetonitrile-water (10: 90, v/v). Then 7 μL of the mixture was injected into the UPLC-Q-TOF/MS system for analysis. Chromatographic separation was performed on an Acquity UPLC HSS T3 column (100 mm × 2.1 mm i.d., 1.8 μm; Waters). The mobile phase was a mixture of 5 mM ammonium acetate containing 0.1% (v/v) formic acid (A) and acetonitrile (B). Gradient elution started

DMD Fast Forward. Published on July 6, 2018 as DOI: 10.1124/dmd.118.081182
This article has not been copyedited and formatted. The final version may differ from this version.

from 5% B, linearly increased to 15% B within 2.5 min, to 20% B within the subsequent 2.5 min, to 32% B in 5 min, and to 90% B in 2 min, maintained for 1 min, and finally adjusted to 5% B for 3 min to re-equilibrate the column. The flow rate was set at 0.4 mL/min, and the column temperature was maintained at 40 °C. The eluent was monitored by UV detection at 300 nm.

MS detection was conducted with electrospray ionization via DuoSpray ion source in positive mode. The parameter settings were as follows: temperature, 500 °C; curtain gas, 40 (arbitrary units); ion source gas 1 and gas 2, 55 (arbitrary units); ion-spray voltage floating, 5.5 kV; and declustering potential, 80 V; collision energy, 10 eV; and collision energy for product ion, 46 eV. The instrument was calibrated before the sample run and automatically calibrated after every five injections. Accurate mass spectra were acquired in the m/z range of 100-1000. Data were acquired via information-dependent acquisition method, which was performed using Analyst TF 1.6.MetabolitePilot™software (AB Sciex), a tool for profiling and characterizing metabolites.

Determination of imrecoxib, M1, M2, and M-CHO. After acetonitrile-induced protein precipitation of samples, 10 μL of the mixture was injected into the liquid chromatography–mass spectrometry (LC-MS/MS) for analysis. The analytes and IS were separated on an Eclipse Plus-C18 column (100 × 4.6 mm i.d., 3.5 μm; Agilent, Santa Clara, CA). Column temperature was maintained at 40 °C. The mobile phase consisted of 5 mM ammonium acetate, formic acid, and acetonitrile (35: 0.1: 65, v/v/v) at the flow rate of 0.7 mL/min. Detection was operated in the positive multiple reaction monitoring (MRM) scan mode by using a dwell time of 100 ms per transition to detect ion pairs at m/z 370 → 236 (imrecoxib), 386 → 236 (M1), 400 → 236 (M2),

DMD Fast Forward. Published on July 6, 2018 as DOI: 10.1124/dmd.118.081182
This article has not been copyedited and formatted. The final version may differ from this version.

384 → 236 (M-CHO), and 386 → 278 (IS). The spray voltage and source temperature were set to 5500 V and 500 °C, respectively.

***In vitro* incubations of imrecoxib and M1.** NADPH (2.0 mM) was pre-incubated with HLM (0.5 mg/mL) or PBS for the control at 37 °C for 10 min; then, 10 μM imrecoxib and M1 were separately added to initiate their individual reactions. After 90 min of incubation, the reactions were terminated by adding an equal volume of ice-cold acetonitrile. For further confirming the participation of CYP enzymes, 10 isoforms of recombinant human CYP enzymes (50 pM), namely, CYP1A2, 2A6, 2B6, 2C8, 2C9, 2C19, 2D6, 2E1, 3A4, and 3A5, were separately incubated with imrecoxib (3.0 μM) in the presence of NADPH for 90 min. The operation procedures and conditions were similar to those for incubation with HLM, except HLMs were replaced by each recombinant human CYP enzyme. The normalized relative contribution of each CYP is calculated according to the method reported previously (Rodrigues, 1999). Incubations of specific-chemical inhibitors (2 μM α-naphthoflavone, 6 μM quercetin, 1 mM ABT, 6 μM sulfaphenazole, 8 μM quinidine, 24 μM ticlopidine, 24 μM clomethiazole, and 2 μM ketoconazole) of each CYP enzyme in HLM with imrecoxib were separately conducted using the similar protocol mentioned above.

For determining the effects of HLC enzymes, HLC (0.5 mg/mL) with or without NAD at 37 °C for 10 min was pre-incubated. Afterward, 10 μM imrecoxib or M1 was added to start the reaction. After 90 min of incubation, the reactions were quenched by the addition of ice-cold acetonitrile.

The metabolism of imrecoxib and M1 was also evaluated in human hepatocytes. Each compound (10 μM) was incubated with human hepatocytes (1.0×10^6 cells/mL)

in WME for 3 h at 37 °C, in the absence or presence of ABT. The reactions were quenched by an equal volume of ice-cold acetonitrile. Each experiment was performed in duplicate.

In *in vitro* incubations, probe substrates (phenacetin, bupropion, paclitaxel, tolbutamide, S-mephenytoin, dextromethorphan, midazolam, testosterone, and SGX523) were selected as positive controls to prove the activity of each enzyme, and the potency and selectivity of the chemical inhibitors.

Trapping of M-CHO in HLM, HLC and recombinant CYPs. Trapping reagent methoxyamine (10 mM) was incubated with NADPH-fortified (2 mM) HLM (0.5 mg/mL) or HLC (0.5 mg/mL). After 10 min of pre-incubation at 37 °C, 10 μM M1 was added to initiate the 90-min reactions, which were terminated using an equal volume of ice-cold acetonitrile. Trapping experiments were also performed to identify the enzyme phenotyping for M-CHO formation, where HLM or HLC was replaced by NADPH-fortified recombinant CYPs. The chromatographic peak areas of M-CHO-methoxyamine adduct detected in CYP incubations were compared with each other.

In vitro **incubations of M-CHO.** M-CHO (10 μM) was selected as the substrate to initiate the reactions, which were conducted similar to the procedure for the *in vitro* incubations of imrecoxib or M1. The incubations included PBS (without or with NAD, NADP, and NADPH), NADPH-fortified HLM, and HLC (with or without NADPH). In addition, for assessing the involvement of aldehyde oxidase (AOX) on the oxidation of M-CHO, specific-chemical inhibitor menadione (20 and 100 μM) was added into HLC incubations. Reaction phenotyping studies of M-CHO were conducted as described for imrecoxib.

M-CHO reduction or oxidation in HLM. 10 μM M-CHO was incubated separately

DMD Fast Forward. Published on July 6, 2018 as DOI: 10.1124/dmd.118.081182
This article has not been copyedited and formatted. The final version may differ from this version.

with recombinant CYP-reductase, human CYP3A4R, and human CYP3A4BLR in the presence of NADPH; these conditions were similar to the protocol for HLM incubations of M-CHO. The effect of α-lipoic acid, a selective inhibitor of CYP-reductase, was conducted at 0, 5, 10, 25, and 50 mM.

Kinetic analysis. In the study, kinetic analyses involved: (a) the conversion of parent to M1 in HLM, (b) its subsequent oxidation to M-CHO in HLM or HLC, (c) conversion of M-CHO to M2 in HLM (c1), HLC (c2) or NADPH-fortified HLC (c3), and (d) competing reduction of M-CHO back to the primary M1 in HLM or NADPH-fortified HLC. For V_{max} and K_m determinations, all substrates (imrecoxib, M1, and M-CHO) were incubated at initial rate in selected concentration ranges, after optimization of incubation time and protein concentrations for the linearity of metabolites formation and < 20% of parent depletion (Table 1).

Nonlinear regression analysis of kinetic data was performed using GraphPad Prism version 6.01 (GraphPad Software, CA, USA). The models fitted included allosteric sigmoidal, substrate inhibition, and Michaelis-Menten. High level of squared correlation coefficient (R^2), as well as appropriate visual inspection of the data, were the goodness-of-fit criteria. CL_{int} values were calculated as V_{max}/K_m, where V_{max} is the maximum velocity, K_m is the Michaelis constant.

Results

Characterization of imrecoxib metabolites in human plasma and urine. A total of 22 metabolites in humans were detected after a single oral administration of 100 mg of imrecoxib (Supplemental Table 1). Metabolic profiles of imrecoxib in human plasma and urine are shown in Fig. 1. M1 and M2 were confirmed using reference standards. In plasma, M1 and M2 were the major circulating substances in addition to the parent drug. The systemic exposure ratio of imrecoxib, M1, and M2 was approximately 1: 1: 4 (Supplemental Table 2). Other minor pathways, such as the hydroxylation of pyrrole and the ω-1 position of N-alkyl chain, were also identified.

Investigation of the metabolism of imrecoxib and M1 *in vitro*. HLM, HLC, and Hepa were selected as the incubation models for exploring the metabolism of imrecoxib *in vitro*. M0 was mostly oxidized to M1 in HLM supplemented with NADPH, and accompanied with minor amounts of M2 which accounted for less than 2% of the total metabolites. The addition of ABT in HLM significantly decreased the formation of the two metabolites by almost 97%, indicating the contribution of CYPs to the conversion. The same phenomenon can be observed in the incubation of M0 with Hepa, where more than 30% of the parent drug was oxidized to M1. By contrast, no metabolites can be detected in HLC incubation with M0, showing that HLC enzymes are not involved in this biotransformation (Fig. 2A).

The formation of M2 originated from the direct conversion of M1 but not of M0, as demonstrated by the limited amount of M2 detected in NADPH-supplemented HLM or Hepa with M0. For investigating this possibility, M1 was incubated in the same *in vitro* systems as M0. Compared with those observed in M0 incubations, M2 yields increased, and M2 can be detected in HLC incubation (Fig. 2B). These observations

DMD Fast Forward. Published on July 6, 2018 as DOI: 10.1124/dmd.118.081182
This article has not been copyedited and formatted. The final version may differ from this version.

confirmed that M2 was generated from M1 instead of M0. However, regardless of the incubation conditions, the M2 yield remains extremely low.

Elucidation on the formation of M-CHO. In general, the metabolic intermediates or metabolites with aldehyde group are always generated when hydroxyl fraction of the compound is oxidized to its corresponding carboxylic acid forms (Diao et al., 2013; Liu et al., 2015; Zhu et al., 2016). Thus, trapping experiments were performed to probe the presence of the aldehyde intermediate. Methoxyamine was used as the trapping agent. A chromatographic peak with the expected $[M + H]^+$ ion at m/z 413.150 (Fig. 3A), and corresponding supportive fragment ions of m/z 381.128, 355.125, and 278.084 (Fig. 3C) were observed when M1 and NADPH-fortified HLM were coincubated with methoxyamine, and a significant decrease in M2 yield relative to that of the incubations in the absence of the trapping agent was observed. The M-CHO-methoxyamine adduct was also detected when the same investigation was conducted with HLC (Fig. 3B). The results confirmed that M1 is oxidized to M-CHO prior to M2 formation in both HLM and HLC incubations.

For exploring the formation of M-CHO, M1 was incubated under different conditions, and the formed M-CHO (m/z 384.2→ 236.2) and M2 (m/z 400.2→ 236.2) were directly detected using LC-MS/MS in MRM scan mode. M-CHO was not able to be detected when M1 was incubated in PBS (Fig. 4A), regardless of the addition of coenzyme NAD, NADP, and NADPH. Meanwhile, no M2 was formed (data not shown). In the NADPH-fortified HLM incubations with M1, M-CHO was observed to accompany the M2 yield (Fig. 4B); upon the addition of ABT, the levels of the two metabolites in HLM markedly decreased (Fig. 4C). In the M1 HLC incubations without NADPH, M2 was detected rather than M-CHO (Fig. 4D), indicating that M-

DMD Fast Forward. Published on July 6, 2018 as DOI: 10.1124/dmd.118.081182
This article has not been copyedited and formatted. The final version may differ from this version.

CHO was immediately oxidized to M2 upon formation. These results showed that CYP and HLC enzymes were both responsible to the M-CHO formation.

Metabolic characteristics of M-CHO. For obtaining further insight into M-CHO metabolism, this metabolic intermediate was synthesized to initiate the incubation experiments. An unexpectedly large amount of M2 was generated when M-CHO was incubated with HLC, whereas M2 together with M1 was considerably formed in NADPH-fortified HLM incubations (Fig. 5). Moreover, M-CHO was almost depleted in these *in vitro* incubations. By striking contrast, less M1 was metabolized when it was selected as the substrate. Thus, we concluded that in enzymatic catalysis, the generation of M-CHO from M1 is the rate-limiting step for M2 formation. The *in vitro* kinetic study provided more direct evidence (Table 1). CL_{int} values for M1 oxidation to M-CHO were minimal whether in HLM or HLC incubations, and the K_m values of this rate-limiting step were marked higher than those of other metabolic processes.

NADPH-dependent effects in different subcelluar fractions for M2 formation. Interestingly, M1 and M-CHO metabolism are influenced significantly by coenzymes, especially NADPH (Fig. 4E and Fig. 5). In HLC incubations, M-CHO was almost completely biotransformed into M2. However, upon the addition of NADPH in HLC incubations, M2 formation was markedly reduced and accompanied by M1 production (Fig. 5A).

When M-CHO was added to NADPH-fortified HLM incubations, M1 was also detected in addition to M2 at the ratio of 1: 2 (Fig. 5B). However, in NADPH-supplemented PBS incubations with M-CHO, neither M1 nor M2 was detected. These data indicated that M-CHO underwent opposite metabolic reactions, that is, oxidation

versus reduction. In addition, the formation of reductive metabolite M1 in these subcellular fractions was dependent on the presence of the cofactor NADPH.

The formation mechanism of M1 in the incubations of M-CHO with NADPH-supplemented HLM was further investigated. In recombinant NADPH-CYP reductase (POR) incubations, M-CHO was completely metabolized to M1 instead of M2, suggesting that POR was responsible for the reduction of M-CHO to M1. α-Lipoic acid was effective in inhibiting M1 formation when a 10-fold molar excess of the inhibitor over M-CHO was used (Fig. 6), further supporting the role of POR in the reduction of M-CHO in HLM.

In addition, in common NADPH-fortified recombinant human CYP3A4 (containing POR and cytochrome b5) incubation with M-CHO, both M2 and M1 can be detected at the ratio of 36: 1, whereas in human CYP3A4R (without cytochrome b5) and human CYP3A4BLR (containing cytochrome b5 but low POR activity) incubations in the presence of NADPH, a significant decrease in M2 was observed, and large amount of M1 was obtained instead with the generation ratios of M2 and M1 of 0.4: 1 and 0.1: 1, respectively (Fig. 7). The results suggested that the oxidation to M2 and reduction to M1 from M-CHO were two competitive pathways. POR and cytochrome b5 are both indispensable electron transporters for the oxidation effect of CYP enzymes. The integrity of the electron transport chain (ETC) of CYPs might accelerate the M-CHO oxidation pathway, whereas ETC deficiency, such as the low activity of POR or the absence of cytochrome b5, leads to attenuated oxidation and drives the reduction reaction.

The reducing enzyme(s) involved in the formation of M1 from M-CHO in HLC is yet to be characterized, because specific inhibitors of several HLC-reducing enzymes, including ADH, aldo-keto reductase, quinone reductase, and glutathione peroxidase,

DMD Fast Forward. Published on July 6, 2018 as DOI: 10.1124/dmd.118.081182
This article has not been copyedited and formatted. The final version may differ from this version.

cannot inhibit the formation of M1 when M-CHO is incubated in NADPH-supplemented HLC (data not shown).

Identification of oxidative enzymes responsible for the formation of M1, M-CHO, and M2. The formation of M1 is CYP-mediated. For identifying the CYP isoforms, 10 isoforms of recombinant human CYP isozymes were individually incubated with M0. Given that M1 is both the metabolite of M0 and the substrate of M2 in HLM, the same metabolic enzymes might be shared by the two metabolic steps, causing underestimation of M1 yield. Therefore, the reduction of M0 was monitored to calculate the contribution of individual human CYP enzymes under the condition that the other minor metabolic pathways of M0 were ignored. CYP3A4, CYP2D6, and CYP3A5 were identified as the principal catalyzing enzymes (Fig. 8A). After normalization for the relative hepatic abundance of CYP enzymes, the relative contributions of CYP3A4 and CYP2D6 were calculated as 68% and 32%, respectively. Specific chemical inhibition tests also provided further supporting data (Supplemental Figure 1).

The same method was applied to evaluate CYP enzyme(s) catalysis of M-CHO to M2. CYP3A4 was confirmed to be the most active enzyme for M2 formation, followed by CYP2D6, with contributions of 61% and 38%, respectively (Fig. 8B). M2 can be detected when M-CHO is incubated with HLC. Aldehyde dehydrogenase (ALDH), AOX, and xanthine oxidase (XO) are the main oxidases for aldehyde compounds in liver cytosol. XO always catalyzes the metabolism of endogenous substances or purine analogs, whereas the structure of imrecoxib and its metabolites do not meet the requirement. In addition, ALDH was non-effective for oxidation in the absence of NADP, whereas M-CHO could be depleted in HLC without any cofactors. Thus, XO and ALDH were disregarded in this experiment. Specific

inhibitor was added in HLC to only identify the possible AOX being responsible for M2 formation. The yield of M2 in HLC was attenuated by up to 25% and 95% by 20 and 100 μM menadione, an AOX inhibitor, respectively. The data indicated that AOX was the most efficient enzyme involved in the formation of M2 in HLC.

To determine which CYP enzyme(s) preferentially oxidize M1 to M-CHO, we performed trapping experiments and investigated the formation of M-CHO adduct in different recombinant human CYP enzymes. The results indicated that CYP3A4, CYP2D6, and CYP3A5 were the key CYP enzymes responsible for the formation of M-CHO, with the ratio of 2:6:1. However, the contributions of the three CYPs might be overestimated, because these isoforms can also catalyze further oxidation of M-CHO. In the HLC incubations with M1, M-CHO cannot be detected, because the formation rate of M2 was considerably higher than that of M-CHO. As a result, the cytosolic enzyme(s) responsible for the oxidation of M1 to M-CHO cannot be identified.

Investigation of M2 formation in rats. To characterize M2 formation *in vivo*, imrecoxib, M1 and M-CHO were directly administered by intravenous injection (i.v.) to SD rats, respectively. The mean plasma concentration-time curves of M2 are presented in Supplemental Figure 2. Following i.v. administration of M-CHO, M1 and imrecoxib, peak plasma concentrations were reached at 0.083, 0.5 and 1 h postdose with mean values of 1013, 902 and 437 ng/mL. The $AUC_{0\text{-}10}$ values were comparable with 1073, 1193 and 736 ng·h/mL, respectively.

Discussion

The carboxylic acid metabolite M2 appears to be the major metabolite of imrecoxib in plasma and urine, accounting for 68% of the systemic exposure and 77% for the total clearance, respectively. However, M2 is not generated to any significant extent in typical *in vitro* metabolic models, including HLM, HLC, and Hepa. The key process for the M2 formation is expected to be found.

The origin of M2 should be defined first because the end-stage metabolite may be directly generated from the parent drug (Xie et al., 2013; Mu et al., 2014); or undergo successive multistep metabolic pathways (Zhou et al., 2015). In the present study, the major metabolic pathway of imrecoxib was characterized as M0 being successively oxidized to M1, to M-CHO, and ultimately to M2, because more M2 was observed in the M1 incubations relative to M0 incubations, and trapping experiments with methoxyamine provided further evidence. The kinetic analyses indicated that the biotransformation from M1 to M-CHO was the rate-limiting step for M2 generation. On the contrary, in *in vivo* conditions, the formation of M2 was comparable after i.v. administration of imrecoxib, M1 and M-CHO, suggesting that the barrier of M-CHO formation was easy to overcome under dynamic and physiological situations. Thus, the discrepancy between *in vivo* and *in vitro* for M-CHO formation may be the key point for explaining why only minor amounts of M2 were formed during *in vitro* incubation of imrecoxib.

NADPH is often used as a cofactor in *in vitro* metabolism investigations for donating electrons. NADPH participates in the oxidation or the reduction based on the electron transport. In NADPH-fortified HLM incubations with M-CHO, the oxidative metabolite M2 could be detected as well as the reductive metabolite M1. The phenomenon also emerged in recombinant CYP3A4 incubations. In general, most

marketed recombinant human CYP enzymes always contain NADPH-POR and cytochrome b5 to enhance the activity of enzymes because the two components are the major electron transporters of ETC (Aigrain et al., 2011; Kenaan et al., 2011). Meanwhile, POR can directly mediate the one-electron reductive biotransformation, such as the nitro reduction of aristolochic acid (Henderson et al., 2003; Stiborova et al., 2005; Stiborova et al., 2011). In the present study, POR can catalyze the reduction of M-CHO back to M1. Compared with CYP3A4 incubation, M2 production significantly decreased with the increase in M1 in human CYP3A4R and CYP3A4BLR incubations with M-CHO. Therefore, it was inferred that the NADPH-dependent POR expressed dual effects, including both oxidation and reduction on M-CHO in HLM by donating electrons to microsomal CYPs or directly to the substrate M-CHO. M1 incubation in NADPH-fortified HLM generated M-CHO which can be further oxidized to M2 and reduced back to M1 simultaneously in two competitive pathways.

In HLC, M-CHO was rapidly metabolized with AOX mediation to M2, whereas in NADPH-fortified HLC, a significant decrease existed in M2 formation. Holm et al. reported that JWH-018, a marketed synthetic cannabinoid, can be oxidized to JWH-018 ω–COOH in HLC, whereas the process can be nearly terminated completely by adding NADPH (Holm et al., 2016). However, the authors did not explain the cause of preventing by this cofactor. As seen in the present study, M-CHO can be reduced back to M1 in HLC in the presence of NADPH, causing the attenuation of the oxidation to M2. However, the NADPH-dependent enzyme(s) in HLC responsible for the M-CHO reduction remains to be identified.

Drugs containing benzylic carbon motif are prone to be oxidized to its corresponding benzylic alcohol (Mamidi et al., 2014; Ryu et al., 2014), and/or

furtherly to the end-product carboxylic acids in *in vivo* (Hvenegaard et al., 2012; Walles et al., 2013; Pozo et al., 2015). In the metabolic process from alcohol to carboxylic acid, it is recognized that there is an aldehyde intermediate, and some *in vitro* trapping tests with methoxyamine or semicarbazide also gave the convincing evidence (Li et al., 2014; Inoue et al., 2015; Liu et al., 2015). However, the further metabolism of aldehyde intermediates is rarely reported in publications. Dopamine is a special case which undergoes oxidative deamination initially to aldehyde (3,4-dihydroxyphenylacetaldehyde, DOPAL), followed by ALDH-mediated oxidation to phenylacetic acid metabolite and reductases-mediated reduction to phenylethanol metabolite (Jinsmaa et al., 2009). Different from M-CHO, DOPAL was reduced to a new forward metabolite, not its precursor dopamine.

In vitro metabolism incubations (such as subcellular fractions) occur in a static system, representing only a few of several dimensions of a complex *in vivo* system (Wang et al., 2010; Subramanian et al., 2013). Several drugs, such as linezolid and ziprasidone, are metabolized through multiple sequential reactions *in vivo*, whereas in *in vitro* systems can only undergo one or two sequential reactions (Wang et al., 2010), especially when a metabolic intermediate is generated. Furthermore, even if the intermediate M-CHO can be partially reduced to M1 *in vivo*, this reduced product might enter into other subcellular fractions, such as kidney microsomes or cytosol where M1 might be easily oxidized again in the absence of NADPH-dependent cytosolic reductase(s) similar to the liver (Brandon et al., 2003; Marchitti et al., 2008; Argikar et al., 2016). It was further supported by the *in vitro* data. M2 could be generated in M1 incubations with human renal homogenate, as well as rat renal homogenate (Supplemental Figure 3). In rats, peak time of M2 plasma concentrations was gradually postponed after i.v. administration of M-CHO, M1 and imrecoxib, and

no significant difference in plasma exposure of M2 was observed among three groups. These results indicated that the metabolite M1 derived from imrecoxib could circulate continuously into liver or other metabolic organs, and be removed from the body in the form of the end-product M2. By contrast, in static *in vitro* incubations, M1 fails to accomplish a similar process to the dynamic *in vivo* system, and the formed M1 was not reused.

It was observed that M1 and M-CHO could interconvert into each other via oxidation or reduction in HLC, as well as in HLM. However, the two metabolic processes are not real reversible reaction steps, because these conversions occurred under different conditions. In HLMs, the conversion of M1 to M-CHO was catalyzed by CYPs, whereas the reduction of M-CHO to M1 was catalyzed by POR. In HLC, these two metabolic pathways were mediated by NADPH-independent enzymes and NADPH-dependent enzymes, respectively.

Li et al. reported that CYP2C9 was the major enzyme involved in the imrecoxib hydroxylation metabolism, along with CYP2D6 and CYP3A4 (Li et al., 2005). In our study, whether the recombinant human CYP2C9 incubation assays or the HLM inhibition experiment with specific-chemical inhibitor sulfaphenazole, both confirmed that CYP2C9 was not responsible for the oxidation of imrecoxib, as well as M1 and M-CHO.

In conclusion, the current study demonstrated that the extensive oxidative metabolism of imrecoxib occurred primarily on its benzylic carbon motif to generate M1 and M2 by a two-step successive oxidization (Fig. 9). The initial hydroxylation was mainly mediated by CYP3A4 and CYP2D6 with relative contributions of 68% and 32%, respectively, to form M1 in HLM. M1 was then oxidized to M-CHO in HLM and HLC. Meanwhile, this process was the rate-limiting step in the generation

DMD Fast Forward. Published on July 6, 2018 as DOI: 10.1124/dmd.118.081182
This article has not been copyedited and formatted. The final version may differ from this version.

of the end-product M2. Two opposite reactions occurred in the further M-CHO metabolism, namely, rapid oxidation to form M2, which was catalyzed by CYP3A4, CYP2D6, and cytosol enzyme AOX, versus reduction to regenerate M1, which was catalyzed by NADPH-dependent reductase in HLM and HLC, such as CYP reductase; thus, the amount of M2 in static *in vitro* incubations was considerably underestimated. The findings presented one of the explanations for the discrepancy between *in vitro* and *in vivo* metabolic data, and the investigation prompted that the effect of competitive reduction on the static oxidation metabolism should be considered in *in vitro* metabolic experiments.

Acknowledgments

We would like appreciate Mr. Fubao Huang for his kind help on the synthesis of M-CHO reference substance. We also would like thank the clinical staff of the Xijing Hospital affiliated with the Fourth Military Medical University and the volunteers in this clinical study.

Authorship contributions

Participated in research design: Hou, Chen, L. Zhou, Zhang, J. Zhou and Zhong.

Conducted experiments: Hou, J. Zhou and Yu.

Contributed new reagents or analytic tools: Hou, J. Zhou, Yu, Chen, Zhong and Zhang.

Performed data analysis: Hou, Chen and L. Zhou.

Contributed to the writing of the manuscript: Hou, Chen and L. Zhou.

Conflicts of interest

The authors declare no conflicts of interest.

References

Aigrain L, Pompon D, and Truan G (2011) Role of the interface between the FMN and FAD domains in the control of redox potential and electronic transfer of NADPH-cytochrome P450 reductase. *Biochem J* **435:**197-206.

Diao X, Deng P, Xie C, Li X, Zhong D, Zhang Y, and Chen X (2013) Metabolism and pharmacokinetics of 3-n-butylphthalide (NBP) in humans: the role of cytochrome P450s and alcohol dehydrogenase in biotransformation. *Drug Metab Dispos* **41:**430-444.

Feng Z, Chu F, Guo Z, and Sun P (2009) Synthesis and anti-inflammatory activity of the major metabolites of imrecoxib. *Bioorg Med Chem Lett* **19:**2270-2272.

Henderson CJ, Otto DME, Carrie D, Magnuson MA, McLaren AW, Rosewell I, and Wolf CR (2003) Inactivation of the hepatic cytochrome P450 system by conditional deletion of hepatic cytochrome P450 reductase. *J Biol Chem* **278:**13480-13486.

Holm NB, Noble C, and Linnet K (2016) JWH-018 omega-OH, a shared hydroxy metabolite of the two synthetic cannabinoids JWH-018 and AM-2201, undergoes oxidation by alcohol dehydrogenase and aldehyde dehydrogenase enzymes in vitro forming the carboxylic acid metabolite. *Toxicol Lett* **259:**35-43.

Hvenegaard MG, Bang-Andersen B, Pedersen H, Jorgensen M, Puschl A, and Dalgaard L (2012) Identification of the cytochrome P450 and other enzymes involved in the in vitro oxidative metabolism of a novel antidepressant, Lu AA21004. *Drug Metab Dispos* **40:**1357-1365.

Inoue K, Fukuda K, Yoshimura T, and Kusano K (2015) Comparison of the Reactivity of Trapping Reagents toward Electrophiles: Cysteine Derivatives Can Be Bifunctional Trapping Reagents. *Chem Res Toxicol* **28:**1546-1555.

Jinsmaa Y, Florang VR, Rees JN, Anderson DG, Strack S, and Doorn JA (2009) Products of oxidative stress inhibit aldehyde oxidation and reduction pathways in dopamine

catabolism yielding elevated levels of a reactive intermediate. *Chem Res Toxicol* **22:**835-841.

Kenaan C, Zhang H, Shea EV, and Hollenberg PF (2011) Uncovering the role of hydrophobic residues in cytochrome P450-cytochrome P450 reductase interactions. *Biochemistry* **50:**3957-3967.

Li F, Lu J, and Ma X (2014) CPY3A4-mediated alpha-hydroxyaldehyde formation in saquinavir metabolism. *Drug Metab Dispos* **42:**213-220.

Li Q, Huang HH, Dong Y, and Zhong DF (2005) [Investigation on the hydroxylation metabolism of imrecoxib in vitro by using recombinant human CYPs]. *Yao xue xue bao = Acta pharmaceutica Sinica* **40:**912-915.

Liu X, Lu Y, Guan X, Dong B, Chavan H, Wang J, Zhang Y, Krishnamurthy P, and Li F (2015) Metabolomics reveals the formation of aldehydes and iminium in gefitinib metabolism. *Biochem Pharmacol* **97:**111-121.

Mamidi RN, Cuyckens F, Chen J, Scheers E, Kalamaridis D, Lin R, Silva J, Sha S, Evans DC, Kelley MF, Devineni D, Johnson MD, and Lim HK (2014) Metabolism and excretion of canagliflozin in mice, rats, dogs, and humans. *Drug Metab Dispos* **42:**903-916.

Mu P, Zheng M, Xu M, Zheng Y, Tang X, Wang Y, Wu K, Chen Q, Wang L, and Deng Y (2014) N-oxide reduction of quinoxaline-1,4-dioxides catalyzed by porcine aldehyde oxidase SsAOX1. *Drug Metab Dispos* **42:**511-519.

Paulson SK, Hribar JD, Liu NW, Hajdu E, Bible RH, Jr., Piergies A, and Karim A (2000) Metabolism and excretion of [(14)C]celecoxib in healthy male volunteers. *Drug Metab Dispos* **28:**308-314.

Pozo OJ, Ibanez M, Sancho JV, Lahoz-Beneytez J, Farre M, Papaseit E, de la Torre R, and Hernandez F (2015) Mass spectrometric evaluation of mephedrone in vivo human metabolism: identification of phase I and phase II metabolites, including a novel succinyl conjugate. *Drug Metab Dispos* **43:**248-257.

Rodrigues AD (1999) Integrated cytochrome P450 reaction phenotyping - Attempting to bridge the gap between cDNA-expressed cytochromes P450 and native human liver microsomes. *Biochem Pharmacol* **57:**465-480.

Rodrigues AD, Halpin RA, Geer LA, Cui D, Woolf EJ, Matthews CZ, Gottesdiener KM, Larson PJ, Lasseter KC, and Agrawal NG (2003) Absorption, metabolism, and excretion of etoricoxib, a potent and selective cyclooxygenase-2 inhibitor, in healthy male volunteers. *Drug Metab Dispos* **31:**224-232.

Ryu SH, Park BY, Kim SY, Park SH, Jung HJ, Park M, Park KD, Ahn T, Kang HS, and Yun CH (2014) Regioselective hydroxylation of omeprazole enantiomers by bacterial CYP102A1 mutants. *Drug Metab Dispos* **42:**1493-1497.

Sandberg M, Yasar U, Stromberg P, Hoog JO, and Eliasson E (2002) Oxidation of celecoxib by polymorphic cytochrome P450 2C9 and alcohol dehydrogenase. *Br J Clin Pharmacol* **54:**423-429.

Stiborova M, Frei E, Hodek P, Wiessler M, and Schmeiser HH (2005) Human hepatic and renal microsomes, Cytochromes P450 1A1/2, NADPH : Cytochrome P450 reductase and prostaglandin H synthase mediate the formation of aristolochic acid-DNA adducts found in patients with urothelial cancer. *Int J Cancer* **113:**189-197.

Stiborova M, Mares J, Levova K, Pavlickova J, Barta F, Hodek P, Frei E, and Schmeiser HH (2011) Role of cytochromes P450 in metabolism of carcinogenic aristolochic acid I: evidence of their contribution to aristolochic acid I detoxication and activation in rat liver. *Neuroendocrinol Lett* **32:**121-130.

Subramanian M, Paruchury S, Singh Gautam S, Pratap Singh S, Arla R, Pahwa S, Jana S, Katnapally P, Yoganand V, Lakshmaiah B, Mazumder Tagore D, Ghosh K, Marathe P, and Mandlekar S (2013) Characterization of recombinantly expressed rat and monkey intestinal alkaline phosphatases: in vitro studies and in vivo correlations. *Drug Metab Dispos* **41:**1425-1432.

Tang C, Shou M, Mei Q, Rushmore TH, and Rodrigues AD (2000) Major role of human liver microsomal cytochrome P450 2C9 (CYP2C9) in the oxidative metabolism of celecoxib, a novel cyclooxygenase-II inhibitor. *J Pharmacol Exp Ther* **293:**453-459.

Tang C, Shou M, Rushmore TH, Mei Q, Sandhu P, Woolf EJ, Rose MJ, Gelmann A, Greenberg HE, De Lepeleire I, Van Hecken A, De Schepper PJ, Ebel DL, Schwartz JI, and Rodrigues AD (2001) In-vitro metabolism of celecoxib, a cyclooxygenase-2 inhibitor, by allelic variant forms of human liver microsomal cytochrome P450 2C9: correlation with CYP2C9 genotype and in-vivo pharmacokinetics. *Pharmacogenetics* **11:**223-235.

Walles M, Wolf T, Jin Y, Ritzau M, Leuthold LA, Krauser J, Gschwind HP, Carcache D, Kittelmann M, Ocwieja M, Ufer M, Woessner R, Chakraborty A, and Swart P (2013) Metabolism and disposition of the metabotropic glutamate receptor 5 antagonist (mGluR5) mavoglurant (AFQ056) in healthy subjects. *Drug Metab Dispos* **41:**1626-1641.

Wang WW, Khetani SR, Krzyzewski S, Duignan DB, and Obach RS (2010) Assessment of a micropatterned hepatocyte coculture system to generate major human excretory and circulating drug metabolites. *Drug Metab Dispos* **38:**1900-1905.

Xie C, Zhou J, Guo Z, Diao X, Gao Z, Zhong D, Jiang H, Zhang L, and Chen X (2013) Metabolism and bioactivation of famitinib, a novel inhibitor of receptor tyrosine kinase, in cancer patients. *Br J Pharmacol* **168:**1687-1706.

Xu H, Zhang Y, Sun Y, Zhang P, Chu F, Guo Z, Zhang H, and Zhong D (2006a) Metabolism and excretion of imrecoxib in rat. *Xenobiotica* **36:**441-455.

Xu HY, Xie ZY, Zhang P, Sun J, Chu FM, Guo ZR, and Zhong DF (2006b) Role of rat liver cytochrome P450 3A and 2D in metabolism of imrecoxib. *Acta Pharmacol Sin* **27:**372-380.

Zhou L, Pang XY, Xie C, Zhong DF, and Chen XY (2015) Chemical and Enzymatic Transformations of Nimesulide to GSH Conjugates through Reductive and Oxidative Mechanisms. *Chem Res Toxicol* **28:**2267-2277.

Zhu YT, Li L, Deng P, Chen XY, and Zhong DF (2016) Characterization of TPN729 metabolites in humans using ultra-performance liquid chromatography/quadrupole time-of-flight mass spectrometry. *J Pharmaceut Biomed* **117:**217-226.

Footnotes

This research was financially supported by the National Natural Science Foundation of China [No. 81573500] and Strategic Priority Research Program of the Chinese Academy of Sciences [No. XDA 12050306].

Figure Legends

Fig. 1. Metabolic profiles (presented in extracted ion chromatograms) after oral administration of 100 mg imrecoxib. In pooled plasma sample at 1 h postdose (A), in pooled plasma sample at 4 h postdose (B), in pooled urine sample at 0-24 h postdose (C), and the chromatogram of the reference substances of imrecoxib, M1, M2, and M-CHO (D).

Fig. 2. Comparison of the amounts of M1 and M2 formed in different *in vitro* incubations, including NADPH-fortified HLM with or without the addition of CYP inhibitor ABT (left), HLC (middle), and Hepa with or without ABT (right). (A) M0 (10 μM) as the substrate; (B) M1 (10 μM) as the substrate. Each column represents the mean of duplicate incubations. N.D., not detectable. Ctr., control.

Fig. 3. Extract ion chromatograms of M-CHO methoxyamine adduct in NADPH- and methoxyamine-supplemented HLM with M1 (A) and methoxyamine-supplemented HLC with M1 (B), and product ion scan spectrum of M-CHO adduct (C). The inset is the tentative fragmentation pattern.

Fig. 4. Chromatograms of LC-MS analyses of M1 (1.5 μM) metabolism in PBS (A), NADPH-fortified HLM (B), NADPH- and ABT-supplemented HLM (C), HLC (D), and NADPH-fortified HLC (E). Peaks I ~ III represent M1, M-CHO, and M2, respectively.

Fig. 5. Effect of the cofactor NADPH on the metabolism of M-CHO (10 μM) in HLC (A) and HLM (B) incubations. Each column represents the mean of duplicate incubations.

Fig. 6. Effect of α-lipoic acid concentrations on the formation of M1 in the recombinant human CYP reductase (POR) incubation containing M-CHO (10 μM), NADPH, and α-lipoic acid.

Fig. 7. Formation of M1 and M2 in M-CHO incubations with recombinant human CYP reductase (POR), CYP3A4 (containing POR and cytochrome b5), CYP3A4R (without cytochrome b5), and CYP3A4BLR (containing cytochrome b5, but with low POR activity). All incubations were supplemented with NADPH. Data are displayed as the means of two separate samples.

Fig. 8. Incubation of imrecoxib (A) and M-CHO (B) in recombinant human CYP enzymes in the presence of NADPH. Each bar represents the mean of two separate samples.

Fig. 9. Proposed formation mechanism of M1 and M2, the major metabolites of imrecoxib in humans.

Table 1. kinetic analyses for imrecoxib oxidation, M1 oxidation, M-CHO oxidation and reduction in HLM, HLC or NADPH-fortified HLC.

Substrate	Metabolite	Incubation	Protein concentration (mg/mL)	Incubation time (min)	Concentration range (μM)	V_{max} (pmol·min^{-1}·mg protein^{-1})	K_m (μM)	CL_{int} (μL·min^{-1}·mg protein^{-1})
Imrecoxib	M1	HLM (NADPH)	0.02	60	0.01 - 100	296	3.72	79.6
M1	M-CHO	HLM (NADPH)	0.10	60	0.25 - 2500	137	979	0.140
M1	M-CHO	HLC	0.10	60	0.25 - 2500	33.9	1299	0.0261
M-CHO	M1	HLM (NADPH)	0.04	45	0.01 – 100	725	8.01	90.5
M-CHO	M2	HLM (NADPH)	0.04	45	0.01 – 100	2780	56.9	48.9
M-CHO	M2	HLC	0.04	45	0.01 – 30	209	1.30	161
M-CHO	M1	HLC (NADPH)	0.02	10	0.01 - 100	973	1.34	727
M-CHO	M2	HLC (NADPH)	0.02	10	0.01 - 100	39195	430	91.2

DMD Fast Forward. Published on July 6, 2018 as DOI: 10.1124/dmd.118.081182
This article has not been copyedited and formatted. The final version may differ from this version.

Figures

Fig.1

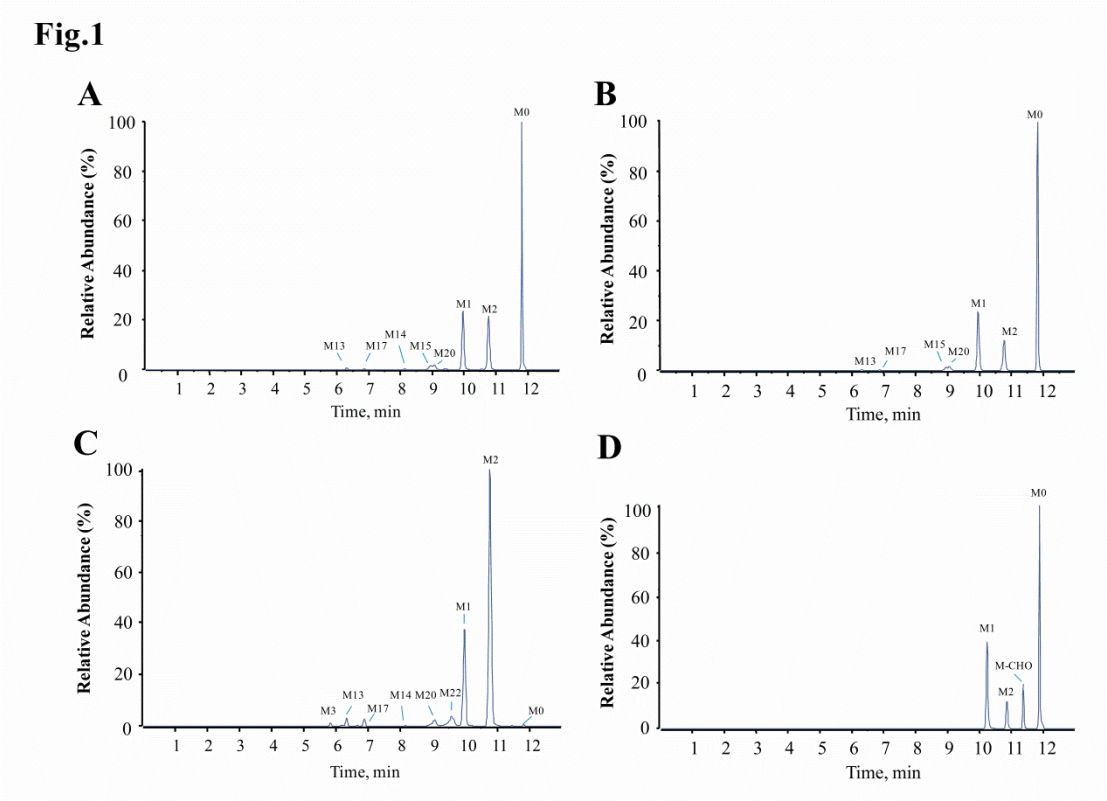

DMD Fast Forward. Published on July 6, 2018 as DOI: 10.1124/dmd.118.081182
This article has not been copyedited and formatted. The final version may differ from this version.

Fig. 2

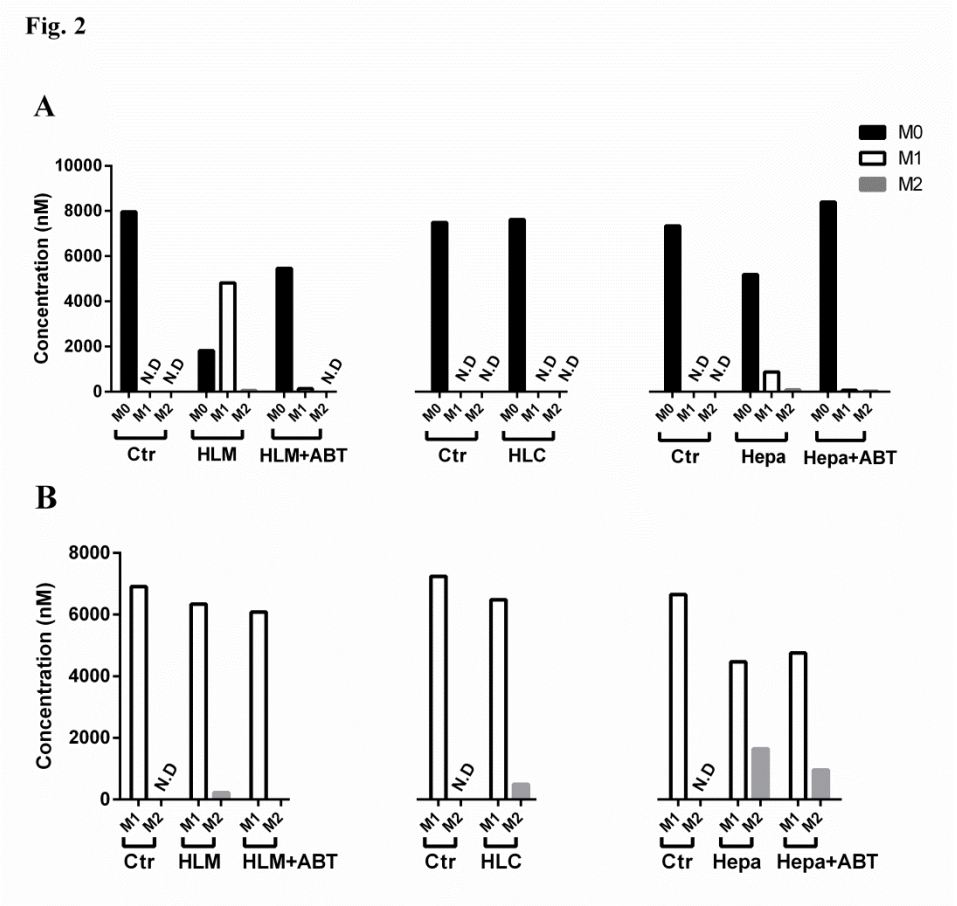

DMD Fast Forward. Published on July 6, 2018 as DOI: 10.1124/dmd.118.081182
This article has not been copyedited and formatted. The final version may differ from this version.

Fig.3

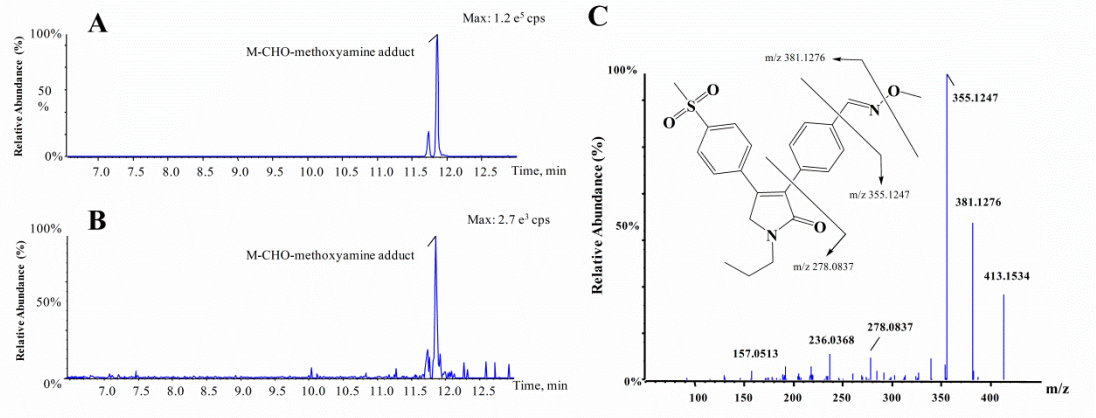

DMD Fast Forward. Published on July 6, 2018 as DOI: 10.1124/dmd.118.081182
This article has not been copyedited and formatted. The final version may differ from this version.

Fig.4

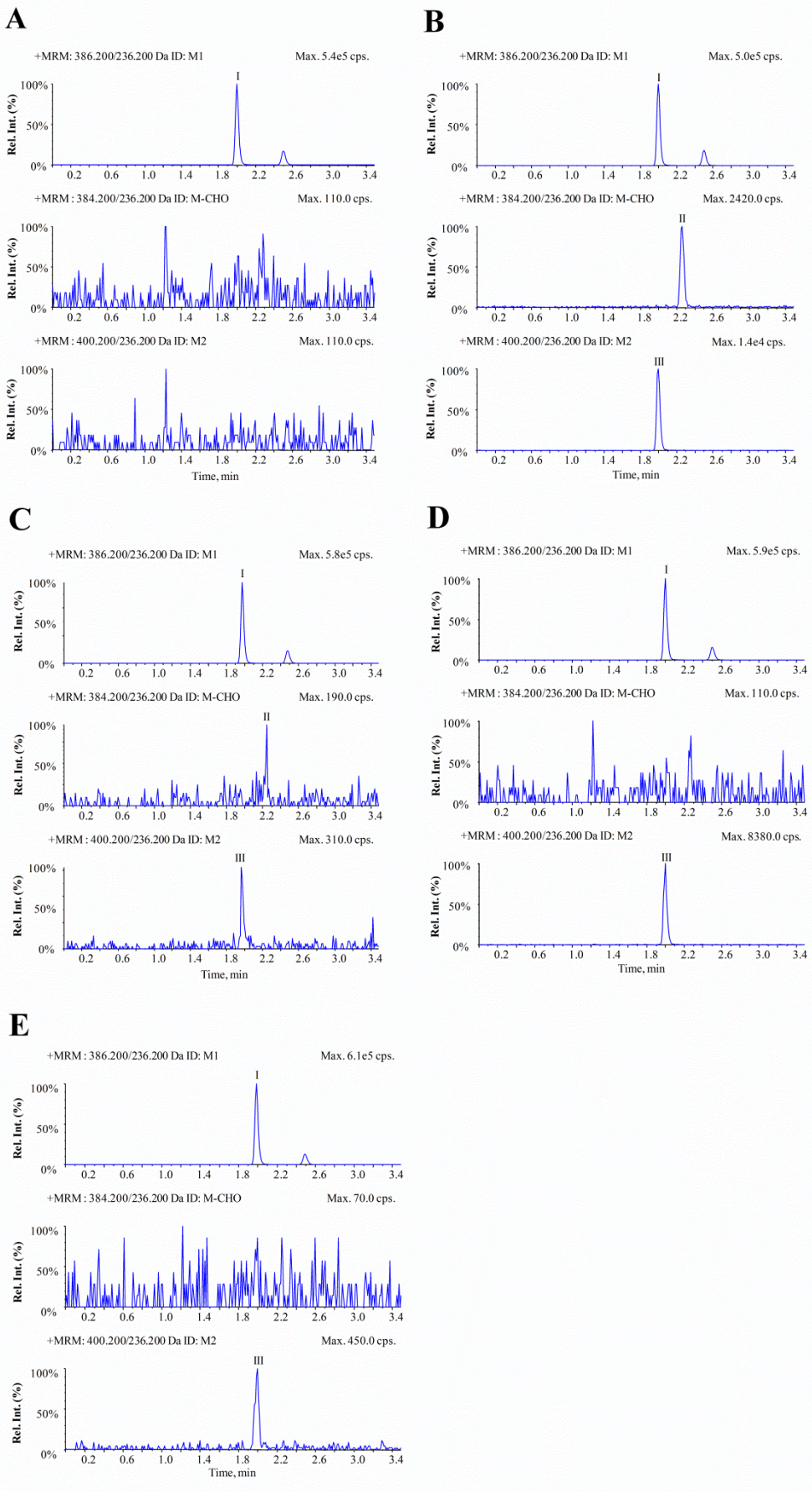

DMD Fast Forward. Published on July 6, 2018 as DOI: 10.1124/dmd.118.081182
This article has not been copyedited and formatted. The final version may differ from this version.

Fig. 5

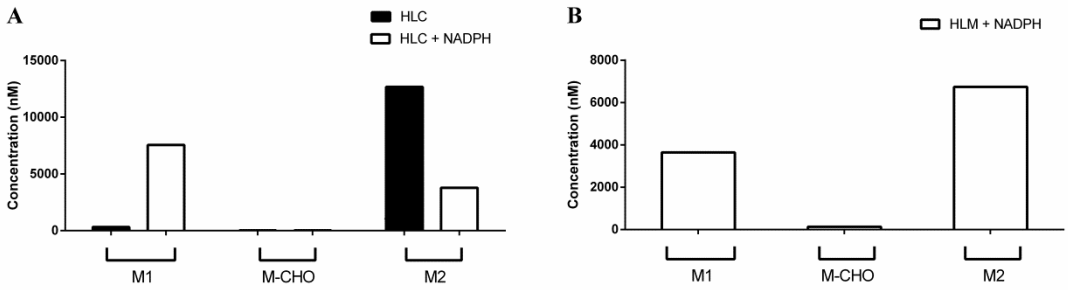

DMD Fast Forward. Published on July 6, 2018 as DOI: 10.1124/dmd.118.081182
This article has not been copyedited and formatted. The final version may differ from this version.

Fig. 6

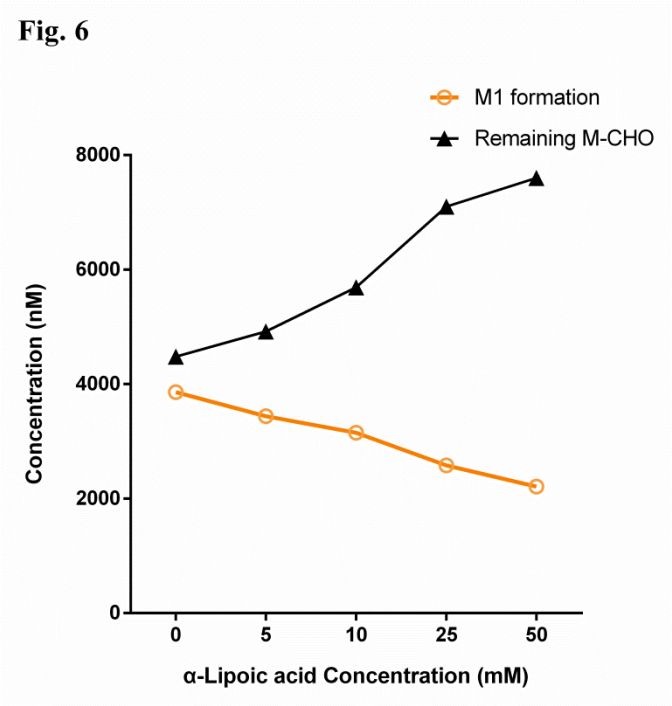

DMD Fast Forward. Published on July 6, 2018 as DOI: 10.1124/dmd.118.081182
This article has not been copyedited and formatted. The final version may differ from this version.

Fig. 7

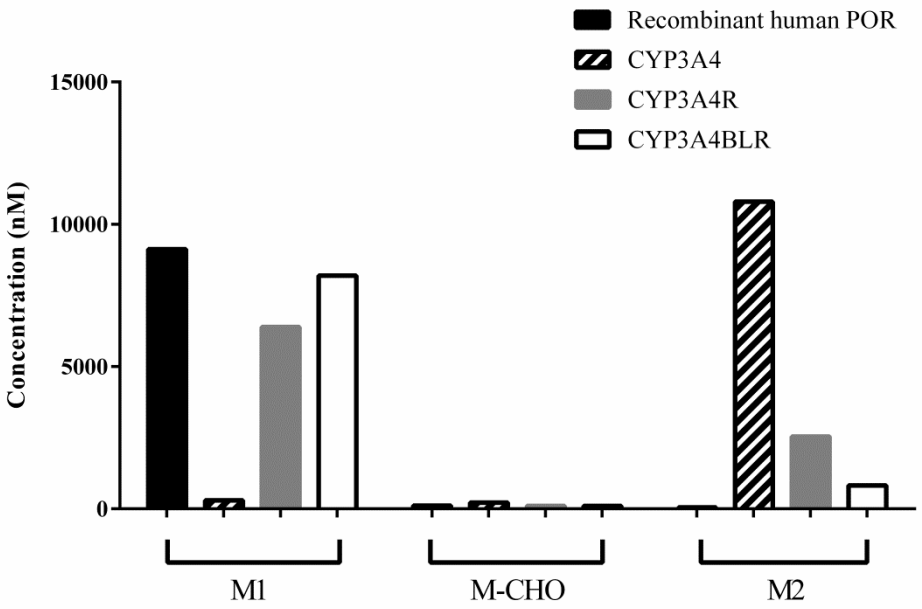

DMD Fast Forward. Published on July 6, 2018 as DOI: 10.1124/dmd.118.081182
This article has not been copyedited and formatted. The final version may differ from this version.

Fig. 8

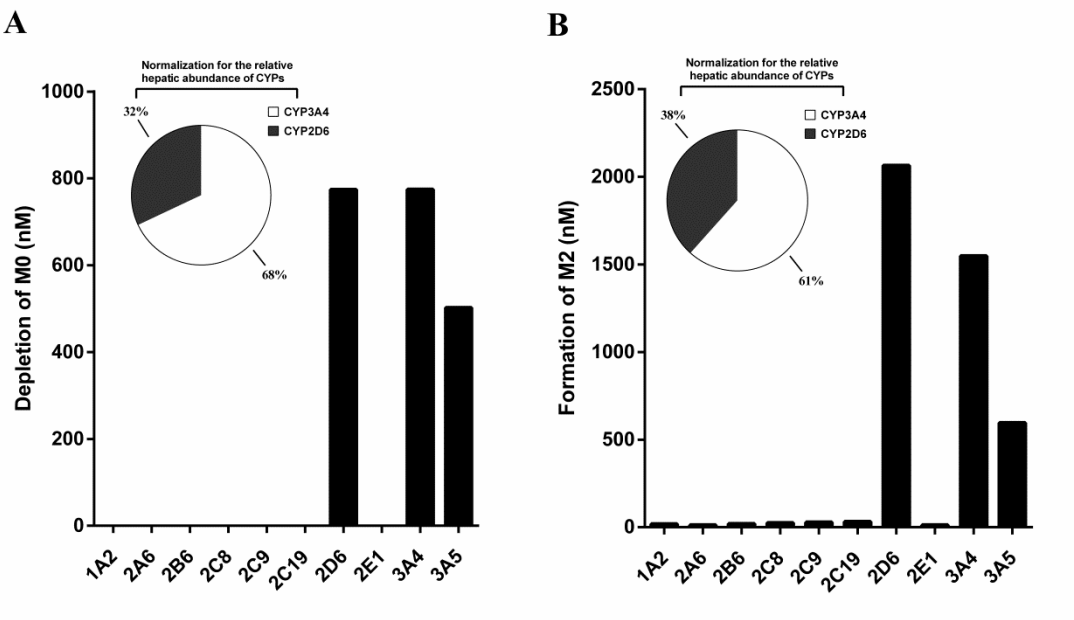

DMD Fast Forward. Published on July 6, 2018 as DOI: 10.1124/dmd.118.081182
This article has not been copyedited and formatted. The final version may differ from this version.

Fig.9